Crack detection in RC structural components using a collaborative data fusion approach based on smart concrete and large-area sensors

Austin Downey, Antonella D'Alessandro, Filippo Ubertini, Simon Laflamme

Austin Downey, Antonella D'Alessandro, Filippo Ubertini, Simon Laflamme, "Crack detection in RC structural components using a collaborative data fusion approach based on smart concrete and large-area sensors," Proc. SPIE 10598, Sensors and Smart Structures Technologies for Civil, Mechanical, and Aerospace Systems 2018, 105983B (27 March 2018); doi: 10.1117/12.2296695

SPIE.

Event: SPIE Smart Structures and Materials + Nondestructive Evaluation and Health Monitoring, 2018, Denver, Colorado, United States

Crack detection in RC structural components using a collaborative data fusion approach based on smart concrete and large-area sensors

Austin Downey[a,c], Antonella D'Alessandro[b], Filippo Ubertini[b], and Simon Laflamme[c,d]

[a]Department of Mechanical Engineering Iowa State University, Ames, IA, USA
[b]Department of Civil and Environmental Engineering, University of Perugia, Perugia, Italy
[c]Department of Civil, Construction, and Environmental Engineering, Iowa State University, Ames, IA, USA
[d]Department of Electrical and Computer Engineering, Iowa State University, Ames, IA, USA

ABSTRACT

Recent advances in the fields of nanocomposite technologies have enabled the development of highly scalable, low-cost sensing solution for civil infrastructures. This includes two sensing technologies, recently proposed by the authors, engineered for their high scalability, low-cost and mechanical simplicity. The first sensor consists of a smart-cementitious material doped with multi-wall carbon nanotubes, which has been demonstrated to be suitable for monitoring its own deformations (strain) and damage state (cracks). Integrated to a structure, this smart cementitious material can be used for detecting damage or strain through the monitoring of its electrical properties. The second sensing technology consists of a sensing skin developed from a flexible capacitor that is mounted externally onto the structure. When deployed in a dense sensor network configuration, these large area sensors are capable of covering large surfaces at low cost and can monitor both strain- and crack-induced damages. This work first presents a comparison of the capabilities of both technologies for crack detection in a concrete plate, followed by a fusion of sensor data for increased damage detection performance. Experimental results are conducted on a $50 \times 50 \times 5$ cm^3 plate fabricated with smart concrete and equipped with a dense sensor network of 20 large area sensors. Results show that both novel technologies are capable of increased damage localization when used concurrently.

Keywords: Carbon nanotubes, Smart cement, Sensor network, Composites damage detection, Structural health monitoring, Sensors, Smart sensors, Smart Structures.

1. INTRODUCTION

The automated detection of cracks in reinforced concrete (RC) components is an important capability for the various stakeholders of civil infrastructure, including owners, operators, consultants, and contractors. Various non-destructive evaluation (NDE) and testing methods exist for crack detection in concrete structures. Currently, visual inspections are the primary method for evaluating the condition of RC components.[1] While visual inspections of structures can often provide sufficient diagnostic information, they tend to be labor-intensive. In addition, visual inspections are not suitable for the detection of defects that occur inside a concrete member[2] or in locations inaccessible to inspectors (e.g. nuclear power facilities[3]). In recent years, the use of visual inspection has been enhanced through the use of automated camera systems and the development of the associated algorithms for crack detection.[4,5] While in many cases these systems provide a marked improvement over traditional visual inspections, their use requires the setup of sometimes bulky equipment and are less suited to the continuous monitoring of structures. In addition to the visual inspection techniques discussed here, other automated or semi-automated systems for the detection and localization of cracks in RC components have been studied. These include ground penetrating radar,[6] ultrasonic methods,[7,8] x-ray tomography[9] and acoustic emission-based[9,10] testing methods. These NDE methods, while are well established and understood, can be difficult to deploy for the continuous monitoring of structures.

Further author information: (Send correspondence to Austin Downey: E-mail: adowney2@iastate.edu)

Sensors and Smart Structures Technologies for Civil, Mechanical, and Aerospace Systems 2018,
edited by Hoon Sohn, Jerome P. Lynch, Kon-Well Wang, Proc. of SPIE Vol. 10598, 105983B
 · doi: 10.1117/12.2296695

Another approach to the automation of crack detection is the incorporation of smart technologies that leverage recent advances in the field of nanocomposites. These technologies allow for the development of highly scalable, low-cost sensing solutions for civil infrastructure. In particular, two smart technologies are of interest for the purpose of this study: self-sensing cementitious materials and sensing skins. Self-sensing cementitious materials are formed through the doping of nanocomposite additives, such as multi-wall carbon nanotubes (MWCNTs), and their conditions can be evaluated through the monitoring of their electrical properties.[11] These materials have been investigated for various strain sensing applications including the dynamic,[12,13] static,[14] and transient loading cases.[15,16] In addition to their well-documented strain sensitivity, these materials have also been investigated for their crack detection capability. Teomete has characterized the crack-detection capabilities of cement matrices doped with carbon fibers[17] and steel[18] fillers. Lim et al. demonstrated that an MWCNT/cement composite could be embedded into an RC beam and was capable of detecting cracks.[19] With the same objective of detecting and localizing cracks, the authors have shown that a crack in an RC beam could be better localized through the introduction of a denser contact array.[20] Also, a model-assisted approach for detecting and localizing cracks using a resistor mesh model was developed and demonstrated on an RC beam.[21] The use of the resistor mesh model was then ameliorated through the development of an automated damage detection scheme.[22]

In addition to the previously discussed self-sensing cementitious materials, sensing skins have seen considerable research and show great potential over traditional NDE systems for the continuous and automated detection of cracks in RC structures. Sensing skins are thin electronic sheets that mimic the ability of biological skin to detect and localize damage over a structure's global area. Different technologies have been leveraged for the creation of sensing skins, including resistive strain gauges,[23,24] piezoceramic transducers and receivers,[25,26] carbon nanotube thin film strain sensors,[27] capacitor-based sensors,[28] structural carbon nanotube composite skins,[29] and graphitic porous sensor arrays on polyimide.[30] When applied onto the surface of RC structures, sensing skins have demonstrated damage detection and localization capabilities. Hallaji et al. showed that a thin layer of conductive copper paint, when applied to the surface of an RC beam, could be used to detect and localize damage through monitoring the skin's change in electrical resistivity.[31] Zhang et al. developed a sensing skin using conductive silver wires printed on either side of a polyester resin sheet and demonstrated its applicability for detecting, localizing, and tracking cracks in RC members.[29] With a specific focus on the low-cost monitoring of large-scale structures, the authors have developed a novel large-area electronic sensor termed the soft elastomeric capacitor (SEC).[32] The SEC forms the basis of a previously proposed and experimentally validated fully-integrated sensing skin.[33] The SEC was designed to be inexpensive and benefits from an easily scalable manufacturing process. The SEC has been studied numerically and experimentally for low-cycle fatigue counts in steel members[34] and for the monitoring of high-cycle fatigue crack growth, intended for the application of monitoring fatigue cracks in steel bridges.[35]

The smart technologies discussed here have different strengths and weaknesses. This work first presents a comparison of the technologies' capabilities for crack detection in a concrete plate. Subsequently, a method for the fusion of sensor data between the two systems that allows for increased damage detection performance is introduced. Experimental results are conducted on a $50 \times 50 \times 5$ cm^3 plate fabricated with smart concrete and equipped with a dense sensor network of 20 large area sensors. Results show that the fusion of data from both novel sensing technologies increases the damage localization potential when compared to a single sensing technology (e.g., self-sensing cementitious material or sensing skin).

2. BACKGROUND

This section provides background on each sensing technology. First, the self-sensing cementitious material is introduced, followed by the SEC-based sensing skin.

2.1 Self-Sensing Cementitious Material

The self-sensing cementitious material used in this work was developed by D'Alessandro et al.[36] Only key concepts related to the material, its fabrication process, and sensing principles are reviewed here for brevity. For more information, the interested reader is referred to reference.[36] The self-sensing cementitious material consists of a cement matrix doped with MWCNT which provides the cement-based composite with increased conductivity (reduced resistivity), the capability to detect damage in the form of changing resistance, and piezoresistive strain

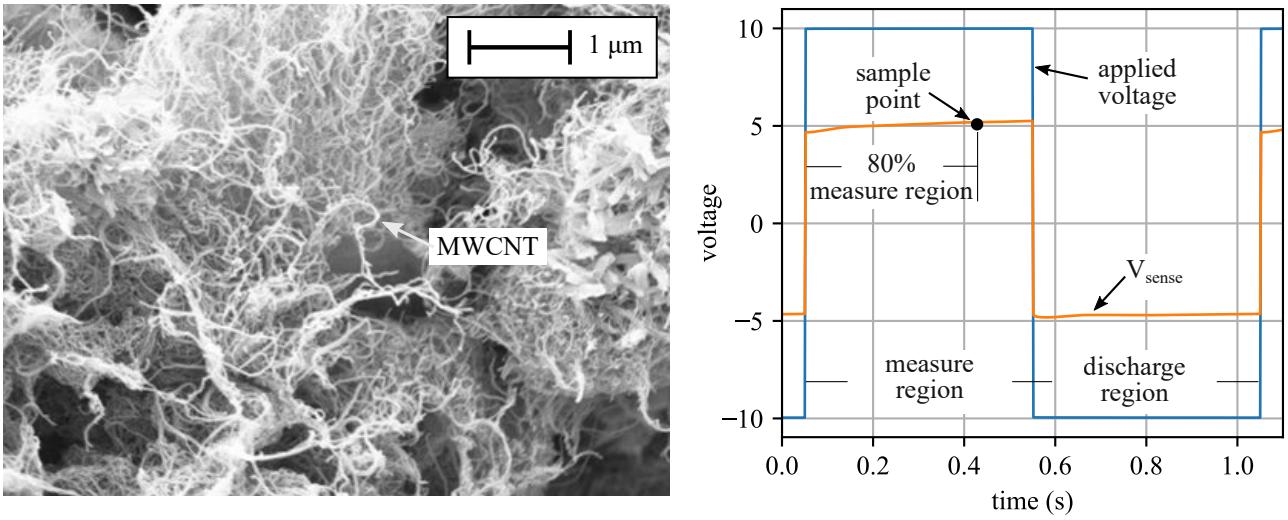

(a) (b)

Figure 1. MWCNT doped multifunctional cement-paste showing: (a) a scanning electron microscope image of MWCNT in the cement-paste matrix; and (b) the biphasic DC measurement approach used for monitoring the plates' electrical characteristics.

sensing properties.[37] For the purpose of this study, a specimen was developed by adding 1% MWCNT (Arkema C100), with respect to the mass of cement, to the cementitious material. The MWCNTs embedded in the cement matrix can be observed in the scanning electron microscope image presented in Figure 1(a). First, the nanotubes were dispersed into the water through sonication. This process was assisted through the use of a surfactant solution of a high molecular weight block copolymer with pigment affinic groups. The nano-modified water suspension was added to the cement and mechanically mixed to form a cement-paste. This paste was then poured into a $50 \times 50 \times 5$ cm^3 mold with two steel reinforcement grids of 6×6 cm^2 with 1.2 mm wire stacked such that their wires and holes aligned. Next, 56 1.2 mm copper contacts were inserted 4 cm into the uncured smart-cement-paste. However, only 36 of these were utilized during experimental testing. These 36 contacts were arranged on a grid of 8×8 cm^2. The unutilized contacts were placed along the perimeter between the utilized contacts. The specimen cured for 28 days before testing.

The measured electrical response of carbon-doped cementitious materials exhibits a temporal drift, often expressed as an increase in the materials resistance measurement with time.[16,36–39] This polarization effect found in carbon-doped smart cement pastes can be circumvented through the use of the biphasic measurement approach that was recently proposed by the authors.[38] The biphasic measurement approach allows for the temporal multi-channel monitoring of self-sensing cementitious material by removing the material's polarization effect. The biphasic measurement approach works by constantly charging and discharging the material to be measured by means of a periodic measure/discharge sensing current in the form of an alternating square wave. Here, the square wave (20 volts peak-to-peak and 50% duty cycle) is sourced from a signal generator. Each cycle of the periodic signal consists of two regions, a "measure region" and a "discharge region", as shown in Figure 1(b). During the discharge region the material depolarization is obtained while a DC voltage measurement is made during the measure region. The DC voltage measurement is taken after 80% of the measure region is completed: this is annotated as the sample point in Figure 1(b).

A resistor mesh model for damage detection, localization and quantification of damage in self-sensing cementitious materials has been proposed by the authors[21] along with an automated scheme for the placement of damage resistors into the resistor mesh model.[22] The resistor mesh model, as proposed, consists of a 2-D mesh of resistors (intended to mimic the electrical response of the smart-cement-paste) and nodes (for voltage measurements at embedded contacts) and is constructed to mimic the conductive specimen's geometry. Once constructed, the resistor mesh model can be solved using nodal analysis. Solving the nodal analysis problem is easily automated using SPICE,[40] an open-source analog electronic circuit simulator. The capability of the

resistor mesh model to detect and localize damage is based on the assumption that damage manifests itself as an increase in resistance in the plate. This increase in resistance is due to the property that cracks in the self-sensing material are considered to cause a reduction in conductivity as they can be considered non-conductive when opened.[12,20,41] Therefore, damage in the plate can be localized through the correct placement of damage (high value) resistors into the resistor mesh model.

The placement of damage resistors into the resistor mesh model requires the definition of an optimization objective function that seeks to reduce the error between the plate's condition and the resistor mesh model. This error can be expressed in terms of type I (false positive) or type II (false negative) errors.[22,42] A simple approach to this problem would be to reduce the occurrence of type I errors by taking the spatially averaged absolute difference of the voltage error between the plate's measured voltage and the model's estimated voltage for each node in the system. While computationally simple, this could lead to a solution with a few single points of high disagreement (i.e. type II error). Therefore, it is important to define a multi-optimization objective function that is capable of being expressed as a single objective optimization function while still being able to find solutions that lie close to the Pareto frontier. This study uses a straightforward scalarization approach, borrowed from the field of robust design,[43] to form a single objective optimization function. The selected approach seeks to find the minimum of a weighted combination of the two objective functions. These are defined as MAE($\mathbf{R}$) for the average error at each contact and $\beta(\mathbf{R})$ for the error value corresponding to the point of maximum disagreement. A scalarization parameter (α) is selected based on the desired trade-off between the two objectives, allowing for a single objective problem for optimizing the selection of a resistor set $\mathbf{R}$ to be formulated as

$$\begin{aligned} \underset{\mathbf{R}}{\text{minimize}} \quad & \text{fit} = (1-\alpha)\frac{\text{MAE}(\mathbf{R})}{\text{MAE}'} + \alpha\frac{\beta(\mathbf{R})}{\beta'} \\ \text{subject to} \quad & \mathbf{R} = [r_1 ... r_m]^{\mathrm{T}} \in \mathbb{R} \\ & 0 \leq \alpha \leq 1 \end{aligned} \tag{1}$$

where MAE$'$ and β' are factors used for normalizing MAE($\mathbf{R}$) and $\beta(\mathbf{R})$. These factors are obtained by solving the resistor mesh model for an initial resistor set that minimizes the current draw error. Once solved, the normalizing factors can be defined as $\text{MAE}' = \text{MAE}(\mathbf{R}_{\text{initial}})$ and $\beta' = \beta(\mathbf{R}_{\text{initial}})$.

The automated placement of high-value resistors into the resistor mesh model has been automated using a sequential Monte Carlo algorithm.[22] This algorithm follows three basic steps: 1) an initial constant value (parent) for each resistor value in the resistor mesh model is obtained; 2) a set of offsprings are randomly sampled from the parent and the fit for each offspring is calculated; 3) the best performing offspring (i.e. the offspring with the lowest level of fit) is selected as the new parent and the cycle is repeated for a predefined number of generations. For a more detailed explanation of the sequential algorithm, including pseudo code and an investigation of parameters, the interested reader is referred to reference.[22]

2.2 SEC-Based Sensing Skin

The SEC, as shown in Figure 2, forms the basis of a previously proposed and experimentally validated sensing skin.[33] The SEC is an inexpensive and robust large-area electronic that is easy to fabricate and highly scalable due to the simplicity of its manufacturing process.[32] The SEC sensor is a parallel plate capacitor, as shown in Figure 2(a), where the dielectric is composed of a styrene-ethylene-butadiene-styrene (SEBS) block co-polymer matrix filled with titania (TiO_2). Titania is used to increase both the durability and permittivity of the dielectric layer. Conductive plates are fabricated using a conductive paint made from the same SEBS but filled with carbon black particles. This conductive paint is then painted onto each side of the SEBS matrix. Once the paint has been allowed to dry, copper contacts are added to the conductors on both the top and bottom plates and a thin layer of conductive paint is applied over the copper contacts to ensure a good connection between the copper contacts and the conductors. Being designed as a parallel plate capacitor, the SEC is transduces a change in the monitored substrates area (i.e. strain) into a change in capacitance (ΔC):

$$\Delta C = e_0 e_r \frac{\Delta A}{\Delta h} \tag{2}$$

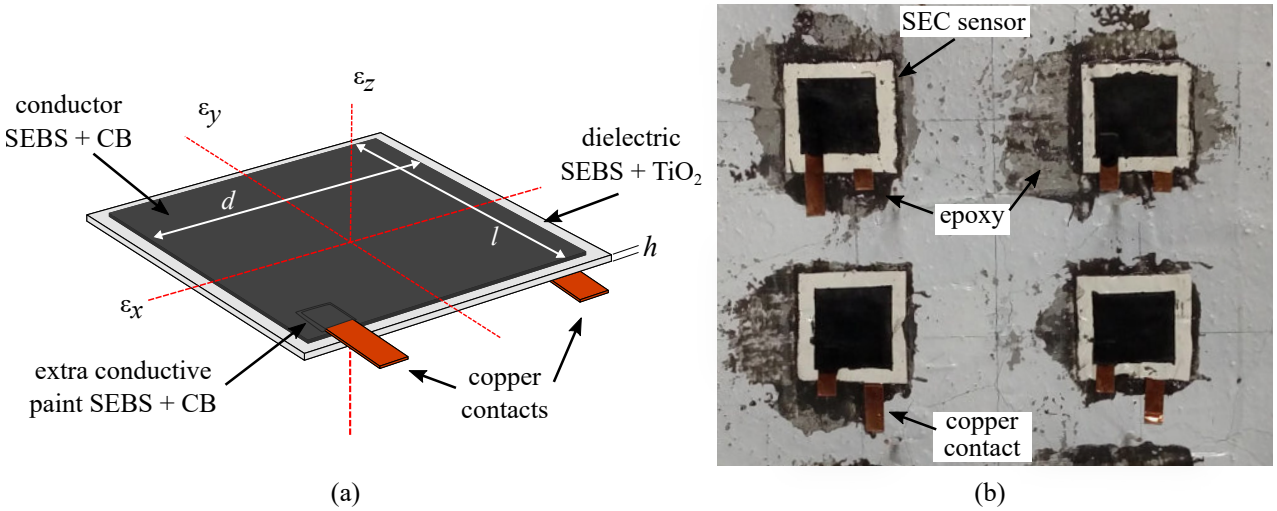

Figure 2. The large area electronic, termed the soft elastomeric capacitor (SEC), used for monitoring the surface condition of the multifunctional cement-paste plate showing: (a) the SEC with its key components labeled and axes annotated; and (b) four SECs deployed onto the cement-paste plate before the connection of wires.

where $e_0 = 8.854$ pF/m is the vacuum permittivity, e_r is the polymer's relative permittivity, $A = d \cdot l$ is the sensor area of width d and length l, and h is the thickness of the dielectric as annotated in Figure 2(a). In addition to its use as a strain transducing sensor,[44] the SEC has also been numerically investigated and validated for the monitoring of fatigue cracks in steel plates. Investigations studied the SEC's capability to detect and localize low-cycle fatigue cracks on compact steel specimens.[34] Additionally, the SEC has also been investigated for the monitoring of high-cycle fatigue cracks, representative of cracking commonly encountered in steel bridges.[35] When deployed in a network, as shown in Figure 2(b), the SEC is capable of detecting and localizing cracks that form under individual sensors. While the capability of the SEC to detect cracks in steel has been studied, the SEC has not been characterized for crack detection in concrete.

3. METHODOLOGY

This section introduces the methodology used for investigating both the self-sensing cementitious material and the SEC-based sensing skin for crack detection in RC structural members. This includes the test setup, the selected model arrangement for the resistor mesh model and the proposed data fusion approach.

3.1 Experimental Test Setup

Experimental validation for the crack detection capability of both the self-sensing cementitious material and the sensing skin were obtained through the testing of the single self-sensing cementitious material plate as shown in Figures 3 and 4. Tests were carried out at the Laboratory of Structural Dynamics at the University of Perugia. The electrical schematic of the test setup, as viewed from the back of the plate, is presented in Figure 3, while the experimental test setup in the lab is shown in Figure 4. The self-sensing cement-paste plate discussed in section 2.1 was mounted vertically in an extruded aluminum frame. A thin white layer of paint was applied to the plate to help in detecting the formation of cracks. For the introduction of cracks into the plate, a 3 kg hammer was mounted on the aluminum frame with a hinge. This hammer was used to provide 100 near identical (rotated back 20° from the vertical) single impacts at the center of the plate. In this presented study, only two conditions of the plate are considered, healthy (no hammer impacts) and damaged (100 hammer impacts).

For the self-sensing cementitious material, a 20 V_{pp} square wave with a frequency of 1 Hz and a 50% duty cycle was sourced from a function generator (DG1022a manufactured by Rigol). This biphasic signal is kept constant throughout the test (e.g., voltage-controlled test). This voltage was applied to the top right of the plate when viewed from the back. The resistor mounted in-line with the sourcing current was used to monitor the plate's total resistance, including the contact resistance at the current input and output contacts.[45] This

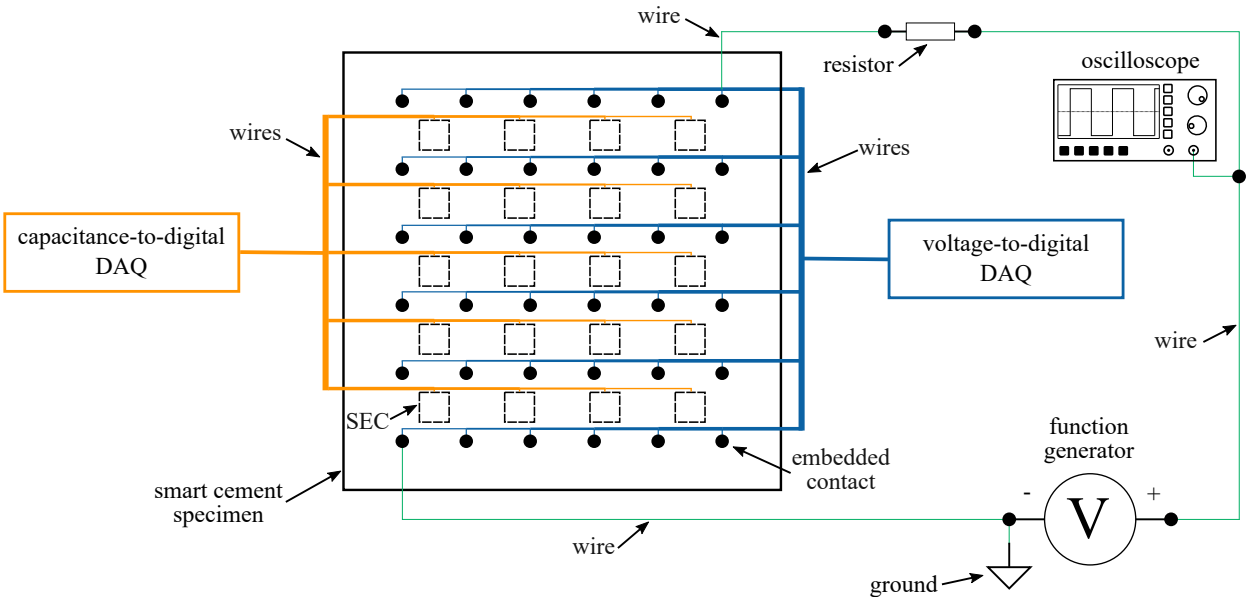

Figure 3. Electrical schematic of the test setup, as viewed from the back, for both the self-sensing cementitious material (monitored through the voltage-to-digital DAQ) and the SEC-based sensing skin (monitored through the capacitance-to-digital DAQ).

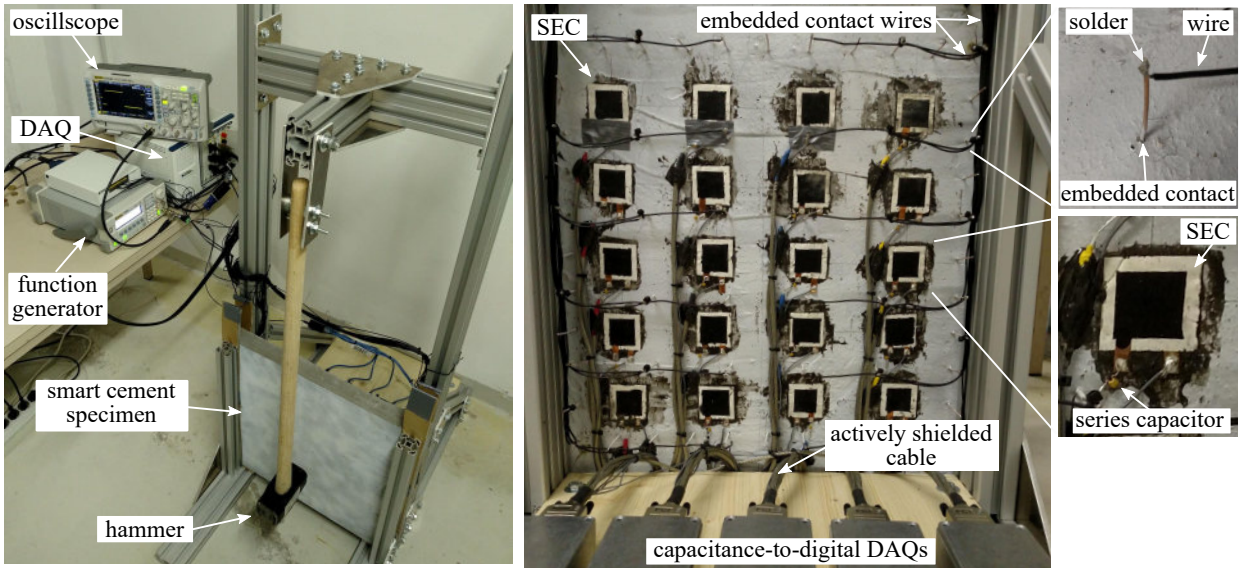

(a) (b)

Figure 4. Experimental test setup showing the: (a) front view of the experimental testing frame used for the impact testing of the self-sensing plate; and (b) back view of the self-sensing plate with the key components annotated and an embedded contact and SEC shown in the inserts.

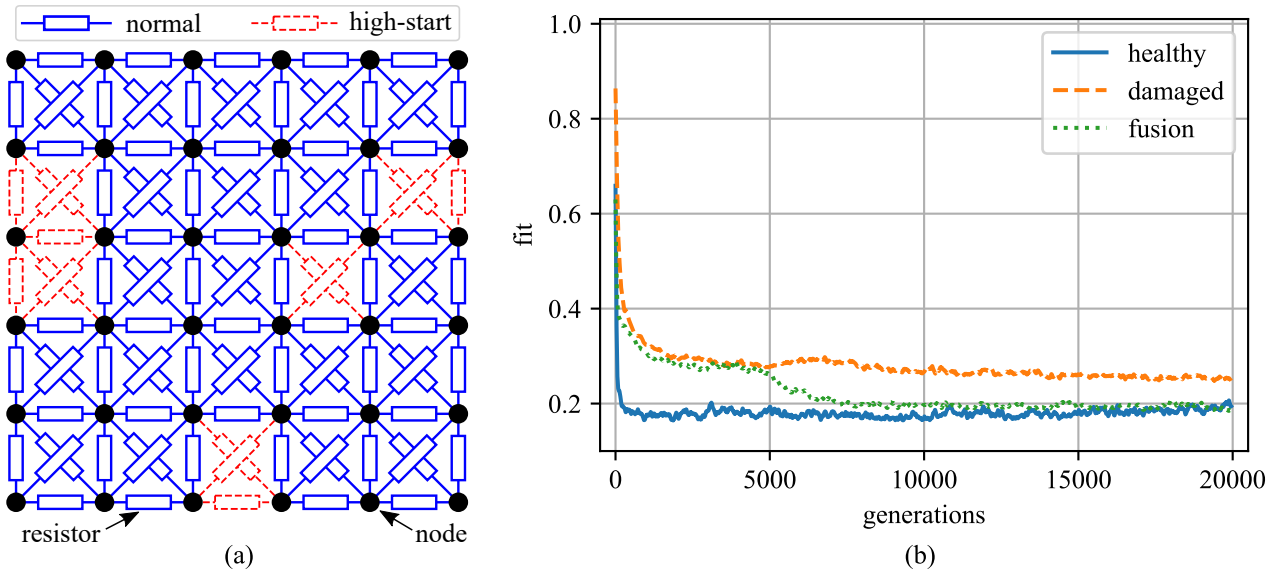

Figure 5. Resistor mesh model used for damage detection: (a) the layout of the resistor mesh model, as viewed from the back of the plate, with the high-start value resistors denoted as resistors with a red dashed outline; and (b) the fit of the resistor mesh model for each generation of the sequential Monte Carlo algorithm.

contact resistance was considered constant throughout the tests and is thus not considered during the placement of damaged resistors. Voltage samples, used as the inputs to the resistor mesh model, were taken using one of two analog input modules: either a 24-bit input module (PXIe-4302) or a 16-bit analog input module (PXIe-6361), both manufactured by National Instruments and mounded in a National Instruments chassis (PXIe-1071). To help ensure a high-quality contact, wires were soldered to the embedded copper contacts. An example is shown in the upper insert of Figure 4(b). Voltage drops were measured at 1 sample per second (S/s), whereby this sampling rate was dictated by the 1 Hz biphasic signal where a DC voltage measurement was made at 80% of the measure region. For validation purposes, an oscilloscope (Rigol DS-1054) was used to monitor the biphasic signal during testing. Parameters used for the sequential Monte Carlo algorithm are discussed in section 3.2.

A 4×5 network of 20 SECs, as shown in Figure 4(b), was deployed onto the back of the concrete plate. Each SEC was individually adhered onto the plate using an off-the-shelf two-part epoxy. The SECs were sampled at 22 S/s using a 16-bit custom-built capacitance-to-digital converter. Each converter (four channels per capacitance-to-digital converter) was held inside a metal project box to limit interference between converters. Capacitance data was recorded over a USB connection from the capacitance-to-digital converter using the same National Instruments chassis used for the analog voltage measurements. Active shielding was used in the cables to remove the cable's parasitic capacitance. This active shielding necessitated the use of a custom triaxial cable, shown in Figure 4(b). The converters can measure up to a maximum of 105 pF. Considering that the SECs had a base capacitance ranging from 100 to 115 pF, a 220 pF ceramic capacitor was added in series to reduce the measured capacitance of each SEC as shown in the lower insert in Figure 4(b). As this capacitance value is not strain sensitive, it does not affect the functionality of the SEC.

3.2 Data Fusion

Here, a simple method for data fusion between the SEC-based sensing skin and the resistor mesh model is proposed. This method is based on the idea that the sequential Monte Carlo algorithm, used for the placement of resistors into the resistor mesh model, will yield better results if it is provided with a better initial guess. Previously, the initial guess for the resistor mesh model was based on the assumption that all resistors in the model started in a healthy state. The values for these healthy resistors were generated through matching the total current flow through the plate to the model's total current flow using a simple gradient descent algorithm. For this study, the initial guess for the sequential Monte Carlo derived damage detection algorithm is obtained from the sensing skin. However, this initial guess could be obtained from any number of NDE methods. The

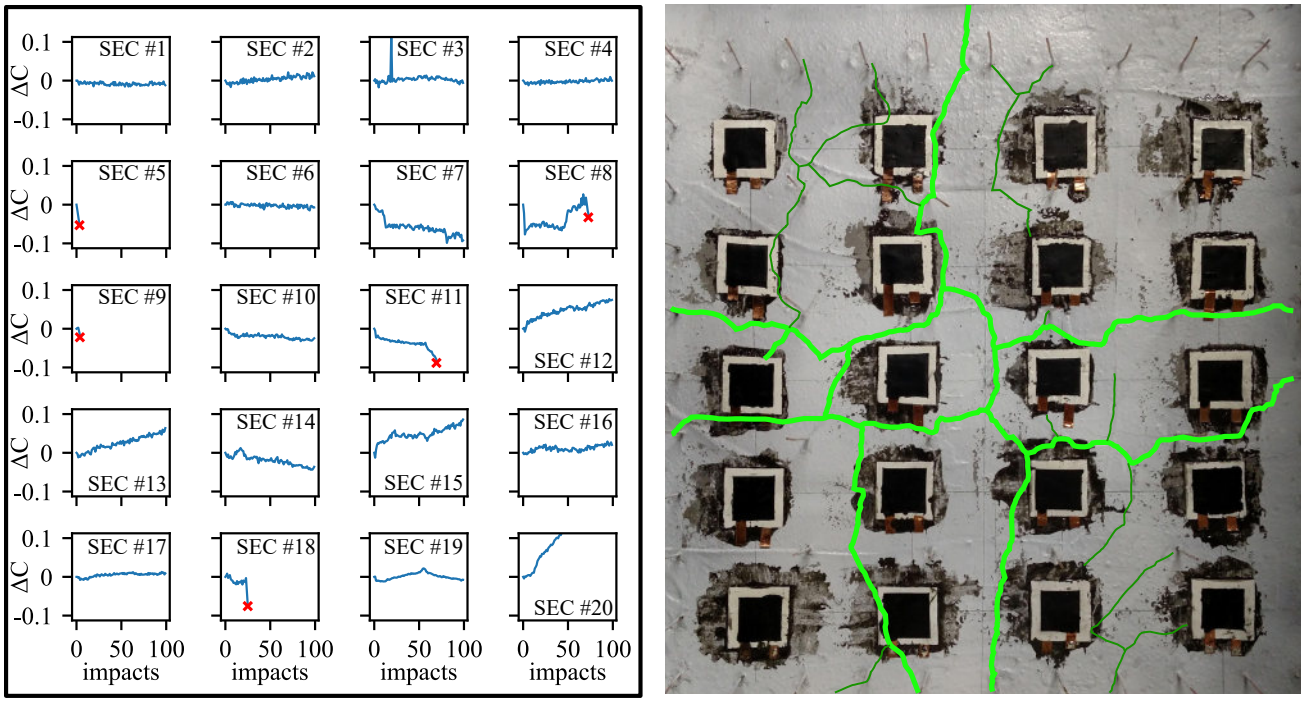

Figure 6. Results for the SEC sensors: (a) expressed as a change in capacitance (ΔC, reported in pF) with sensor debonding being denoted by a red "x"; (b) deployment of the 20 SECs on the back of the cement-paste plate with major (thick light green lines) and minor (thin dark green lines) cracks highlighted.

resistor mesh model used in this study is presented in Figure 5(a). The initial guess is formed through the selection of certain resistors in the resistor mesh model that start in a high-start state as these resistors have a higher probability of being damaged than those in the rest of the plate. These high-start resistors are presented in Figure 5(a) as resistors with a dashed red outline. Because the SECs are capable of monitoring an area for crack growth, any resistors in the resistor mesh model that are covered by, or close to, the SEC are used as high-start values resistors. Additionally, because of the nature of the algorithm, a resistor that starts in a high resistance state may not finish in a high resistance state. The capability of individual resistors in the resistor mesh model to adjust their resistance values over generations through the sequential Monte Carlo algorithm adds a robustness to the algorithm. Once a high resistance value has been set for these resistors in the first generation of the sequential Monte Carlo algorithm, the algorithm is allowed to run until an end condition has been met (e.g. a low fit value or a set number of generations).

For this study, each sequential Monte Carlo algorithm uses a population of 100, evaluated over 20,000 generations with a dynamic range (the amount by which each resistor is allowed to change over a single generation) of 100 Ω. These parameters were selected through a preliminary investigation by first making educated guesses about the value for the dynamic range and α. Then, the population number and generational count were set to a high level to ensure that the algorithm started to converge to a solution. Additionally, these are the same parameters used in reference,[22] allowing for a convenient comparison with previously published work. The convergence of the three sequential Monte Carlo algorithms used in this work can be seen in Figure 5(b). In this work, the three sequential Monte Carlo algorithms ran are for (i) healthy, (ii) damaged (no data fusion) and (iii) fusion (damaged with data fusion) resistor mesh models. Figure 5(b) shows that the more accurate initial guesses, provided by the sensing skin as high-start resistor values, can help yield a more accurate resistor mesh model fit to the experimental data.

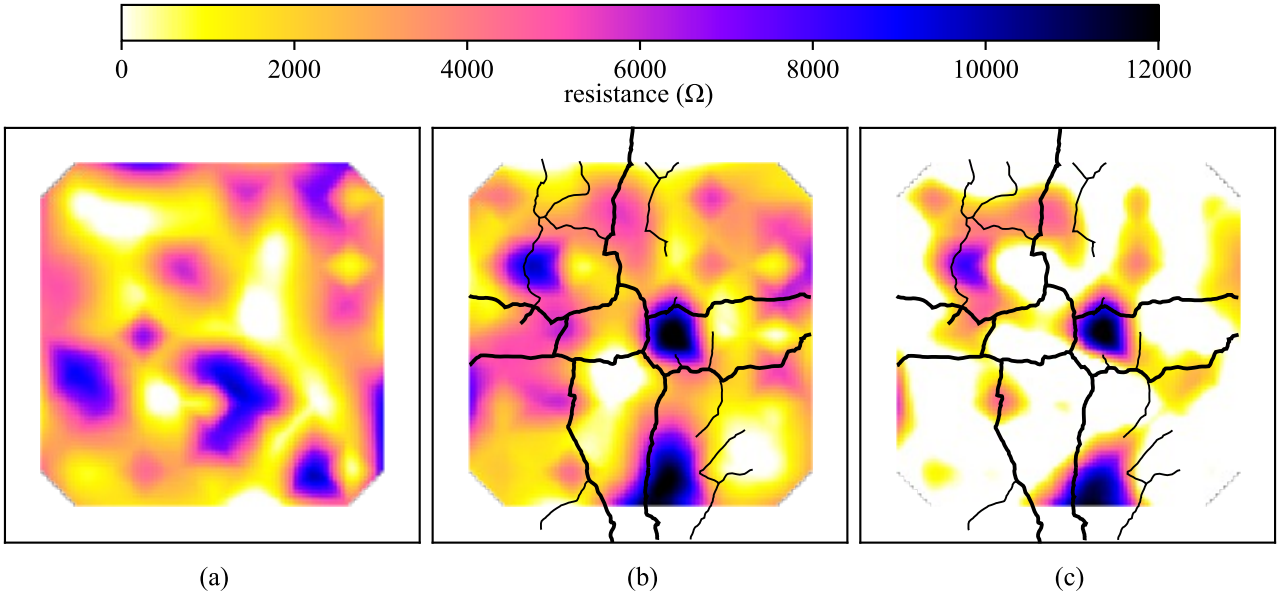

Figure 7. Spatial damage results, viewed from the back of the plate, as solved by the resistor mesh model: (a) resistance values for the healthy plate; (b) resistance values for the plate with 100 impacts with the major (thick black lines) and minor (thin black lines) cracks outlined; and (c) the change in resistance values between the healthy and damaged states.

4. RESULTS

This section first presents a comparison of the technologies' capabilities for crack detection in the concrete plate, followed by the crack detection and localization results for the proposed sensor fusion method.

4.1 SEC-Based Sensing Skin

The spatial and temporal (in terms of impacts) results for the SEC-based sensing skin's crack detection capability are presented in Figure 6. Figure 6(a) reports the spatial and temporal results for each capacitor in terms of its change in capacitance, and Figure 6(b) shows the deployment of the 20 SECs on the back of the plate (with the spatial arrangement corresponding to that of Figure 6(a)). For clarity, an image before the installation of wires is used to show the locations of cracks in the plate's damaged state. The major cracks (cracks that are clearly visible on the front of the plate) are denoted by thick light green lines and minor cracks (cracks only visible on the back of the plate) by thin dark green lines. As illustrated in Figure 6, the capability of a sensing skin to detect cracks is a function of the density of the individual sensors. In this study, the SECs only covered about 10% of the total area inside the outer ring of embedded copper contacts. This percentage excludes the white dielectric that extends past the black conductive plate because it does not contribute to the measurement. This relatively low density, combined with the sensor layout used in this study, resulted in the majority of cracks forming around the SEC sensors. In the cases where large cracks did form under SEC sensors, the combination of the opening of the crack and the impact loading of the hammer caused a debonding between the white paint and the cement-paste. The SECs detached in such a way that the transducer, epoxy, and paint separated from the cement-paste in one piece. This debonding allowed the now separated SEC sensor to contract as it was no longer held in its pretensioned state by the cement-paste substrate. This contraction was recorded as a large drop in capacitance and is recorded in Figure 6(a) as a red "x" for SEC sensors 5, 8, 9, 11, and 18. As the debonding present in these sensors is considered to be a product of large cracks opening under these sensors, these sensors are treated as sensors that detected cracks forming under their respective areas. Therefore, these sensors are used as inputs to determine the location of high-start resistors for the data fusion method presented in section 3.2. A selected set of sensors, 2, 12, 13, 15, 16, 19, and 20 did exhibit an increase in capacitance, a signal that corresponds to the opening of a crack. However, due to uncertainties in relating this change in signal to a quantifiable crack opening, these sensors are not used as inputs for the data fusion method. Future work

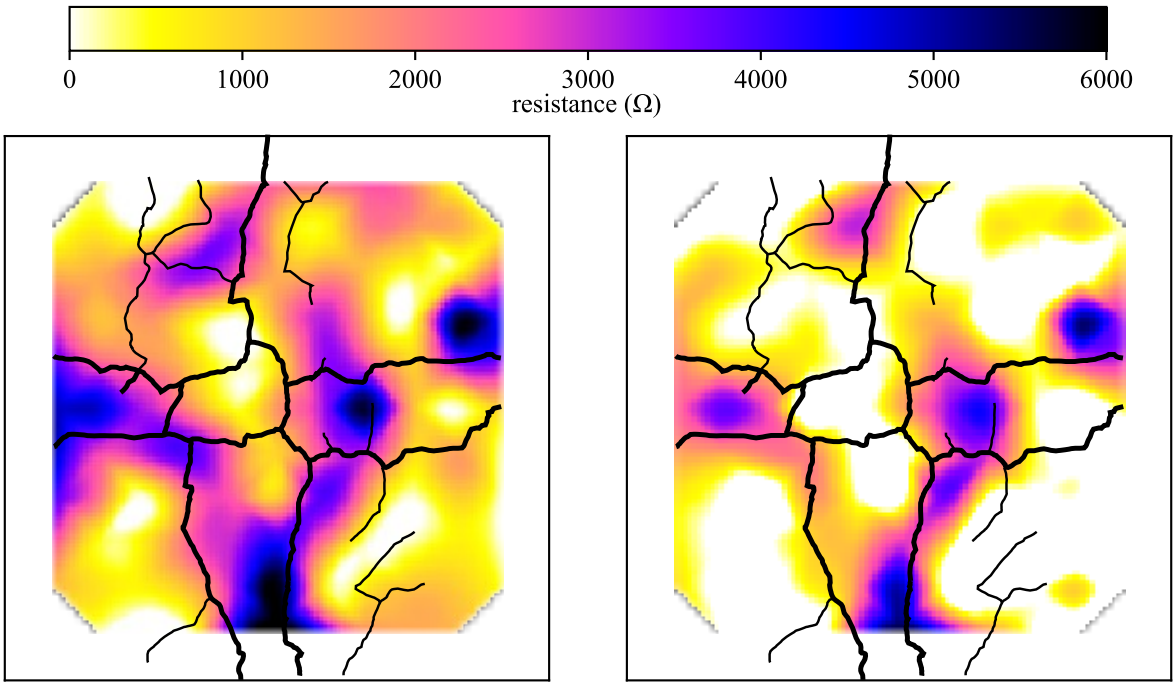

Figure 8. Spatial damage results, as viewed from the back of the plate, from the fusion of the SEC and resistivity data as solved by the resistor mesh model: (a) resistance values for the plate with 100 impacts with the major (thick black lines) and minor (thin black lines) cracks outlined; and (b) the change in resistance values between the healthy and damaged states.

will be required to quantify the link between a change in an SEC's capacitance signal and the opening of a crack in concrete.

4.2 Self-Sensing Cementitious Material

The capability of the self-sensing cementitious material in combination with the sequential Monte Carlo algorithm to locate cracks present in a concrete plate is illustrated in Figure 7. These results were previously reported by Downey et al.[22] Figure 7(a) presents the spatial resistance (i.e. damage) mapping for the healthy condition of the cement-paste plate, as viewed from the back, Figure 7(b) presents the spatial resistance mapping for the damage condition, and Figure 7(c) presents the change in resistance between Figures 7(a) and 7(b). For the selected damage case, the resistor mesh model is able to identify the locations where the damage is most significant. This is due to the sequential Monte Carlo algorithm first solving for the damage locations that are the most evident, therefore making detection of less evident damages more difficult.

4.3 Data Fusion

The fusion of the sensing skin and the resistor mesh model used in conjunction with the self-sensing cementitious material is expressed in Figure 8. Figure 8(a) is the spatial resistance mapping for the resistor mesh model that is solved for using the high-start conditions determined by the sensing skin. Figure 8(b) shows the change in resistance between Figure 8(b) and the healthy state found in Figure 7(a). Generally, the fusion of data between the sensing skin and the resistor mesh model demonstrates a better capability for detecting more of the significant damage found in the plate. This figure, along with Figure 5(b), shows that the resistor mesh model can benefit from the initial guesses provided by the sensing skin.

5. CONCLUSION

This work introduced and reported on a data fusion method for two recently proposed sensing technologies. The first technology consists of a smart-cementitious material doped with multi-wall carbon nanotubes used along a bespoke model assisted damage technique termed the resistor mesh model. The second sensing technology consists of a sensing skin based on a dense network of novel flexible capacitors that are mounted externally on the structure. For the purpose of this study, the SECs are mounded on a specimen (a plate measuring $50 \times 50 \times 5$ cm^3) of self-sensing cementitious material.

This work first showed that the SEC-based sensing skin was capable of detecting cracks that manifested directly under a sensor, but not around. A solution to this shortcoming is the application of a denser array of SEC sensors inside the sensing skin, a solution that would be made easier with a fully integrated sensing skin (e.g., a denser network). In comparison to the sensing skin, the self-sensing cementitious material combined with the previously developed resistor mesh model can detect damage over the continuous plate. However, this method could only detect salient damages and required the use of a time-consuming algorithm to detect and localize damage in the model. Lastly, a method for fusing the two sensing technologies was presented. This data fusion method consisted of detecting and localizing damage using the sensing skin and then using the location of this damage to define a better initial guess for the resistor mesh model. Results showed that the fusion of the data from both novel technologies enhanced the damage localization capability.

Future work on the topic includes: the development of a proper bounding technique for the SEC sensors onto the cement-based materials; the characterization of crack openings in cement-based materials monitored by an SEC; the development of better optimization techniques for the resistor mesh model; the quantification of crack size detection capabilities using the resistor mesh model, and further studying of the proposed data fusion method with the potential of using other nondestructive techniques to obtain initial guesses.

ACKNOWLEDGMENTS

The support of the Italian Ministry of Education, University and Research (MIUR) through the funded Project of Relevant National Interest (PRIN) entitled "SMART-BRICK: Novel strain-sensing nano-composite clay brick enabling self-monitoring masonry structures" (protocol no. 2015MS5L27) is gratefully acknowledged. This work is also partly supported by the National Science Foundation Grant No. 1069283, which supports the activities of the Integrative Graduate Education and Research Traineeship (IGERT) in Wind Energy Science, Engineering and Policy (WESEP) at Iowa State University. This work was also partly supported by the Ministerio de Economía y Competitividad of Spain and the Consejería de Economía, Innovación, Ciencia y Empleo of Andalucía (Spain) under projects DPI2014-53947-R and P12-TEP-2546. E. G-M was also supported by a FPU contract-fellowship from the Spanish Ministry of Education Ref: FPU13/04892.

REFERENCES

[1] Institute, A. C., "201.1r-08 guide for conducting a visual inspection of concrete in service," tech. rep., American Concrete Institute (2008).

[2] Wu, Z., Li, J., Gu, C., and Su, H., "Review on hidden trouble detection and health diagnosis of hydraulic concrete structures," *Science in China Series E: Technological Sciences* **50**, 34–50 (oct 2007).

[3] Perry, M., Yan, Z., Sun, Z., Zhang, L., Niewczas, P., and Johnston, M., "High stress monitoring of pre-stressing tendons in nuclear concrete vessels using fibre-optic sensors," *Nuclear Engineering and Design* **268**, 35–40 (mar 2014).

[4] Prasanna, P., Dana, K. J., Gucunski, N., Basily, B. B., La, H. M., Lim, R. S., and Parvardeh, H., "Automated crack detection on concrete bridges," *IEEE Transactions on Automation Science and Engineering* **13**(2), 591–599 (2016).

[5] Dawood, T., Zhu, Z., and Zayed, T., "Machine vision-based model for spalling detection and quantification in subway networks," *Automation in Construction* **81**, 149–160 (sep 2017).

[6] Eisenmann, D., Margetan, F. J., Koester, L., and Clayton, D., "Inspection of a large concrete block containing embedded defects using ground penetrating radar," in [*43rd Review of Progress in Quantitative Nondestructive Evaluation*], AIP Publishing LLC (2016).

[7] Clayton, D. A., Smith, C. M., Ferraro, D. C. C., Nelson, J., Khazanovich, D. L., Hoegh, D. K., Chintakunta, S., and Popovics, D. J., "Evaluation of ultrasonic techniques on concrete structures," tech. rep., Oak Ridge National Laboratory (ORNL) (2013).

[8] Breysse, D., "Nondestructive evaluation of concrete strength: An historical review and a new perspective by combining NDT methods," *Construction and Building Materials* **33**, 139–163 (aug 2012).

[9] Suzuki, T., Ogata, H., Takada, R., Aoki, M., and Ohtsu, M., "Use of acoustic emission and x-ray computed tomography for damage evaluation of freeze-thawed concrete," *Construction and Building Materials* **24**, 2347–2352 (dec 2010).

[10] Chen, B. and Liu, J., "Damage in carbon fiber-reinforced concrete, monitored by both electrical resistance measurement and acoustic emission analysis," *Construction and Building Materials* **22**, 2196–2201 (nov 2008).

[11] Han, B., Zhang, L., and Ou, J., "Self-sensing concrete," in [*Smart and Multifunctional Concrete Toward Sustainable Infrastructures*], 81–116, Springer Singapore (2017).

[12] Azhari, F. and Banthia, N., "Cement-based sensors with carbon fibers and carbon nanotubes for piezoresistive sensing," *Cement and Concrete Composites* **34**, 866–873 (aug 2012).

[13] Sun, M., Liew, R. J., Zhang, M.-H., and Li, W., "Development of cement-based strain sensor for health monitoring of ultra high strength concrete," *Construction and Building Materials* **65**, 630–637 (aug 2014).

[14] Zhang, H., Hou, S., and Ou, J., "Smart aggregate-based seismic stress monitoring system using a specially designed charge amplifier," *Journal of Intelligent Material Systems and Structures* **27**, 418–426 (oct 2015).

[15] Han, B., Yu, X., and Kwon, E., "A self-sensing carbon nanotube/cement composite for traffic monitoring," *Nanotechnology* **20**, 445501 (oct 2009).

[16] Monteiro, A., Loredo, A., Costa, P., Oeser, M., and Cachim, P., "A pressure-sensitive carbon black cement composite for traffic monitoring," *Construction and Building Materials* **154**, 1079–1086 (nov 2017).

[17] Teomete, E., "Measurement of crack length sensitivity and strain gage factor of carbon fiber reinforced cement matrix composites," *Measurement* **74**, 21–30 (oct 2015).

[18] Teomete, E., "The effect of temperature and moisture on electrical resistance, strain sensitivity and crack sensitivity of steel fiber reinforced smart cement composite," *Smart Materials and Structures* **25**, 075024 (jun 2016).

[19] Lim, M.-J., Lee, H. K., Nam, I.-W., and Kim, H.-K., "Carbon nanotube/cement composites for crack monitoring of concrete structures," *Composite Structures* **180**, 741–750 (nov 2017).

[20] Downey, A., Garcia-Macias, E., D'Alessandro, A., Laflamme, S., Castro-Triguero, R., and Ubertini, F., "Continuous and embedded solutions for SHM of concrete structures using changing electrical potential in self-sensing cement-based composites," in [*Nondestructive Characterization and Monitoring of Advanced Materials, Aerospace, and Civil Infrastructure 2017*], Wu, H. F., Gyekenyesi, A. L., Shull, P. J., and Yu, T.-Y., eds., SPIE (apr 2017).

[21] Downey, A., D'Alessandro, A., Baquera, M., García-Macías, E., Rolfes, D., Ubertini, F., Laflamme, S., and Castro-Triguero, R., "Damage detection, localization and quantification in conductive smart concrete structures using a resistor mesh model," *Engineering Structures* **148**, 924 – 935 (2017).

[22] Downey, A., D'Alessandro, A., Ubertini, F., and Laflamme, S., "Automated crack detection in conductive smart-concrete structures using a resistor mesh model," *Measurement Science and Technology* (dec 2017).

[23] Hu, Y., Huang, L., Rieutort-Louis, W. S. A., Sanz-Robinson, J., Sturm, J. C., Wagner, S., and Verma, N., "A self-powered system for large-scale strain sensing by combining CMOS ICs with large-area electronics," *IEEE Journal of Solid-State Circuits* **49**, 838–850 (apr 2014).

[24] Tung, S.-T. and Glisic, B., "Sensing sheet: the response of full-bridge strain sensors to thermal variations for detecting and characterizing cracks," *Measurement Science and Technology* **27**, 124010 (oct 2016).

[25] Schulz, M. J. and Sundaresan, M. J., [*Smart Sensor System for Structural Condition Monitoring of Wind Turbines: May 30, 2002-April 30, 2006*], National Renewable Energy Laboratory (2006).

[26] Giurgiutiu, V., Zagrai, A., and Bao, J., "Damage identification in aging aircraft structures with piezoelectric wafer active sensors," *Journal of Intelligent Material Systems and Structures* **15**, 673–687 (sep 2004).

[27] Loh, K. J., Hou, T.-C., Lynch, J. P., and Kotov, N. A., "Carbon nanotube sensing skins for spatial strain and impact damage identification," *Journal of Nondestructive Evaluation* **28**, 9–25 (mar 2009).

[28] Sharp, N., Kuntz, A., Brubaker, C., Amos, S., Gao, W., Gupta, G., Mohite, A., Farrar, C., and Mascareñas, D., "A bio-inspired asynchronous skin system for crack detection applications," *Smart Materials and Structures* **23**, 055020 (apr 2014).

[29] Zhang, B., Zhou, Z., Zhang, K., Yan, G., and Xu, Z., "Sensitive skin and the relative sensing system for real-time surface monitoring of crack in civil infrastructure," *Journal of Intelligent Material Systems and Structures* **17**, 907–917 (oct 2006).

[30] Luo, S., Hoang, P. T., and Liu, T., "Direct laser writing for creating porous graphitic structures and their use for flexible and highly sensitive sensor and sensor arrays," *Carbon* **96**, 522–531 (jan 2016).

[31] Hallaji, M., Seppänen, A., and Pour-Ghaz, M., "Electrical impedance tomography-based sensing skin for quantitative imaging of damage in concrete," *Smart Materials and Structures* **23**, 085001 (jun 2014).

[32] Laflamme, S., Kollosche, M., Connor, J. J., and Kofod, G., "Robust flexible capacitive surface sensor for structural health monitoring applications," *Journal of Engineering Mechanics* **139**, 879–885 (jul 2013).

[33] Downey, A., Laflamme, S., and Ubertini, F., "Experimental wind tunnel study of a smart sensing skin for condition evaluation of a wind turbine blade," *Smart Materials and Structures* (Oct 2017).

[34] Kong, X., Li, J., Bennett, C., Collins, W., and Laflamme, S., "Numerical simulation and experimental validation of a large-area capacitive strain sensor for fatigue crack monitoring," *Measurement Science and Technology* **27**, 124009 (oct 2016).

[35] Kong, X., Li, J., Collins, W., Bennett, C., Laflamme, S., and Jo, H., "A large-area strain sensing technology for monitoring fatigue cracks in steel bridges," *Smart Materials and Structures* **26**, 085024 (jul 2017).

[36] D'Alessandro, A., Rallini, M., Ubertini, F., Materazzi, A. L., and Kenny, J. M., "Investigations on scalable fabrication procedures for self-sensing carbon nanotube cement-matrix composites for SHM applications," *Cement and Concrete Composites* **65**, 200–213 (jan 2016).

[37] Han, B., Zhang, K., Yu, X., Kwon, E., and Ou, J., "Electrical characteristics and pressure-sensitive response measurements of carboxyl MWNT/cement composites," *Cement and Concrete Composites* **34**, 794–800 (jul 2012).

[38] Downey, A., D'Alessandro, A., Ubertini, F., Laflamme, S., and Geiger, R., "Biphasic DC measurement approach for enhanced measurement stability and multi-channel sampling of self-sensing multi-functional structural materials doped with carbon-based additives," *Smart Materials and Structures* **26**, 065008 (may 2017).

[39] Wong, I., Loh, K. J., Wu, R., and Garg, N., "Effects of ultra-low concentrations of carbon nanotubes on the electromechanical properties of cement paste," in [*Nanotechnology in Construction*], 371–376, Springer International Publishing (2015).

[40] Paolo Nenzi, H. V., [*Ngspice Users Manual - Version 26*], Paolo Nenzi, Holger Vogt, USA (2014).

[41] Wang, S. and Chung, D., "Self-sensing of flexural strain and damage in carbon fiber polymer-matrix composite by electrical resistance measurement," *Carbon* **44**, 2739–2751 (nov 2006).

[42] Flynn, E. B. and Todd, M. D., "A bayesian approach to optimal sensor placement for structural health monitoring with application to active sensing," *Mechanical Systems and Signal Processing* **24**, 891–903 (may 2010).

[43] Doltsinis, I. and Kang, Z., "Robust design of structures using optimization methods," *Computer Methods in Applied Mechanics and Engineering* **193**, 2221–2237 (jun 2004).

[44] Laflamme, S., Ubertini, F., Saleem, H., D'Alessandro, A., Downey, A., Ceylan, H., and Materazzi, A. L., "Dynamic characterization of a soft elastomeric capacitor for structural health monitoring," *Journal of Structural Engineering* **141**, 04014186 (aug 2015).

[45] Han, B., Guan, X., and Ou, J., "Electrode design, measuring method and data acquisition system of carbon fiber cement paste piezoresistive sensors," *Sensors and Actuators A: Physical* **135**, 360–369 (apr 2007).